Chemical Senses, 2018, Vol 43, 357–366
doi:10.1093/chemse/bjy022
Original Article
Advance Access Publication 6 April 2018

OXFORD

Original Article

A Multispecific Investigation of the Metal Effect in Mammalian Odorant Receptors for Sulfur-Containing Compounds

Ruina Zhang[1,*], Yi Pan[1,*], Lucky Ahmed[2], Eric Block[3], Yuetian Zhang[1], Victor S. Batista[2] and Hanyi Zhuang[1,4]

[1]Department of Pathophysiology, Key Laboratory of Cell Differentiation and Apoptosis of the Chinese Ministry of Education, Shanghai Jiaotong University School of Medicine, 227 South Chongqing Road, Huangpu District, Shanghai 200025, P. R. China, [2]Department of Chemistry, Yale University, 225 Prospect Street, New Haven, CT 06520, USA, [3]Department of Chemistry, University at Albany, State University of New York, 1400 Washington Avenue Albany, NY 12222, USA and [4]Institute of Health Sciences, Shanghai Jiaotong University School of Medicine/Shanghai Institutes for Biological Sciences of Chinese Academy of Sciences, 320 Yueyang Road, Xuhui District, Shanghai 200031, P. R. China

*These authors contributed equally to the work.

Correspondence to be sent to: Hanyi Zhuang, Department of Pathophysiology, Key Laboratory of Cell Differentiation and Apoptosis of the Chinese Ministry of Education, Shanghai Jiaotong University School of Medicine, Shanghai 200025, P. R. China. e-mail: hanyizhuang@sjtu.edu.cn and Victor S. Batista, Department of Chemistry, Yale University, New Haven, CT 06520, USA. e-mail: victor.batista@yale.edu

Editorial Decision 15 March 2018.

Abstract

Metal-coordinating compounds are generally known to have strong smells, a phenomenon that can be attributed to the fact that odorant receptors for intense-smelling compounds, such as those containing sulfur, may be metalloproteins. We previously identified a mouse odorant receptor (OR), Olfr1509, that requires copper ions for sensitive detection of a series of metal-coordinating odorants, including (methylthio)methanethiol (MTMT), a strong-smelling component of male mouse urine that attracts female mice. By combining mutagenesis and quantum mechanics/molecular mechanics (QM/MM) modeling, we identified candidate binding sites in Olfr1509 that may bind to the copper–MTMT complex. However, whether there are other receptors utilizing metal ions for ligand-binding and other sites important for receptor activation is still unknown. In this study, we describe a second mouse OR for MTMT with a copper effect, namely Olfr1019. In an attempt to investigate the functional changes of metal-coordinating ORs in multiple species and to decipher additional sites involved in the metal effect, we cloned various mammalian orthologs of the 2 mouse MTMT receptors, and a third mouse MTMT receptor, Olfr15, that does not have a copper effect. We found that the function of all 3 MTMT receptors varies greatly among species and that the response to MTMT always co-occurred with the copper effect. Furthermore, using ancestral reconstruction and QM/MM modeling combined with receptor functional assay, we found that the amino acid residue R260 in Olfr1509 and the respective R261 site in Olfr1019 may be important for receptor activation.

Key words: ancestral reconstruction, copper, odorant receptors, orthologs, sulfur

Introduction

Odorant receptors (ORs) are members of the G protein-coupled receptor superfamily that have 7 transmembrane domains and respond to exogenous odorants (Buck and Axel 1991; Firestein 2001; Duan et al. 2012). The binding of a certain odorant to a specific OR is determined by the structure and the concentration of the odorous ligand in the nasal mucus, as well as by the specificity of the odorant–OR interaction at the binding site (Araneda et al. 2000; Katada et al. 2005; Touhara and Vosshall 2009; Nagashima and Touhara 2010; Persaud et al. 2013). Good metal-coordinating ligands, such as amines and thiols, can be detected by the olfactory system at very low concentrations (Laska et al. 2007), possibly due to the fact that metal ions and nanoparticles (particularly copper and zinc) may enhance the binding between ORs and these ligands. Different studies have predicted the role of metals in olfaction (Crabtree 1978; Wang et al. 2003; Viswaprakash et al. 2009; Vodyanoy 2010; Moore et al. 2012; Block et al. 2017). We previously identified the mouse OR, Olfr1509, as a receptor for (methylthio)methanethiol (MTMT), which is a sulfur-containing compound in mouse urine that plays an important role in mating (Lin et al. 2005; Duan et al. 2012). More importantly, we found that copper ions could significantly enhance the function of Olfr1509 when responding to MTMT. Electrophysiological recordings of the mouse septal organ (SO) neurons, where Olfr1509 is prominently expressed, and a behavioral assay corroborated the role of copper in MTMT response and perception, effectively validating the aforementioned hypothesis that ORs can function as metalloproteins (Duan et al. 2012). Furthermore, using site-directed mutagenesis and quantum mechanics/molecular mechanics (QM/MM) calculations, we proposed potential binding sites (H105, C109, and N202) to the copper/MTMT complex in this receptor (Sekharan et al. 2014).

In addition to MTMT, Olfr1509 is responsive toward a range of sulfur-containing compounds including other thiols and sulfides on addition of copper (Duan et al. 2012). In a more recent study, by screening against the human OR repertoire, we characterized the first human receptor with a significant copper effect (Li et al. 2016). We found that OR2T11 could respond to small thiols up to 5 carbons, and the response was enhanced with the addition of copper and silver ions. In this study, we will focus on MTMT as an example of sulfur-containing compounds that require copper, but not any other metals, for the activation of ORs.

Fueled by rapid environmental changes, ORs are one of the fastest evolving gene families (Bozza et al. 2009; Hayden et al. 2010; Zhao et al. 2013; Chatelain et al. 2014; Niimura et al. 2014), with its members frequently becoming pseudogenized, deleted, or duplicated, leading to dramatic changes in olfactory gene repertoires in different species (Niimura and Nei 2007). In addition, sequence variations within individual genes result in dramatic variations of the function of orthologous OR pairs (Conant and Wolfe 2008; Zhuang et al. 2009; Forslund et al. 2011; Nehrt et al. 2011; Adipietro et al. 2012; Altenhoff and Dessimoz 2012; Altenhoff et al. 2012; Chen and Zhang 2012). Previous work has shown that OR orthologs can exhibit diverse functions in different mammalian species (Zhuang et al. 2009; Adipietro et al. 2012). Significant functional changes were seen in different primates' OR7D4/OR7D1 orthologs; furthermore, amino acid residues responsible for the functional changes were obtained by ancestral reconstruction and mutagenesis analysis. Adipietro et al. found that orthologous ORs have similar ligand choices but different response magnitudes, suggesting adaption during evolution.

Here, we investigated the molecular mechanisms of MTMT reception and the OR copper effect by characterizing the functions of orthologous MTMT receptors. Given the high sequence identities of the orthologs of a given OR, comparing the function of orthologs may identify sites vital for function in the OR gene of interest. Indeed, our functional studies revealed dramatic changes among the orthologs of the 2 MTMT receptors with copper effects in different mammalian species. Furthermore, through ancestral reconstruction and functional characterization of the Olfr1509 rodent lineage, we found that the site R260 may be crucial for receptor activation in MTMT receptors with a copper effect. Using QM/MM modeling combined with mutagenesis analysis, we found that R260/R261 is located in the C254/R260/K269 and C203/M254/R261 MTMT/Cu binding pockets in Olfr1509 and Olfr1019, respectively.

Materials and methods

Chemicals

$CuCl_2$ was purchased from Adamas and was dissolved in water. MTMT was synthesized by Dr Eric Block and was dissolved in ethanol. All chemicals were diluted further into working concentrations before experiments.

Genomic DNA

Mammalian genomic DNA was purchased from Zyagen, including cow (*Bos taurus*), rat (*Rattus norvegicus*, Sprague Dawley), Chinese hamster (*Cricetulus griseus*), dog (*Canis familiaris*), guinea pig (*Cavia porcellus*), horse (*Equus caballus*), cat (*Felis catus*), rabbit (*Oryctolagus cuniculus*), and pig (*Sus scrofa*). Primate genomic DNA was purchased from the Coriell Cell Repositories, including chimpanzee (*Pan troglodytes*), gorilla (*Gorilla gorilla*), white-cheeked gibbon (*Hylobates leucogenys*), rhesus macaque (*Macaca mulatta*), pig-tailed macaque (*Macaca nemestrina*), marmoset (*Callithrix jacchus*), and squirrel monkey (*Saimiris ciureus*). Human genomic DNA was extracted from buccal swab cells using the TIANamp Genomic DNA Kit (Tiangen Biotech). Little brown bat (*Myotis lucifugus*) genomic DNA was a generous gift from Dr David A. Ray at Mississippi State University.

Orthologous sequence mining

Mammalian OR orthologs were mined using the mouse Olfr1509, Olfr1019, and Olfr15 nucleotide sequences against the Reference RNA sequence ("Refseq_rna") in the GenBank database. Putative orthologs were defined as the reciprocal best hits to the mouse reference ORs with at least 80% identity. Among the species queried, complete or partial orthologous sequences were found for rat, hamster, guinea pig, rabbit, pig, cow, dog, cat, horse, and human for all 3 receptors. The partial rabbit Olfr1509 sequence from GenBank was BLATed against the rabbit (Assembly OryCun2.0) genome in the Ensembl database to obtain the complete sequence. Sequencing of our polymerase chain reaction (PCR) amplification products verified the presence of all orthologs in all species used.

Ancestral reconstruction

Olfr1509 orthologous ORs from 17 species, including mouse, human, marmoset, cow, rat, Chinese hamster, horse, cat, rabbit, pig, little brown bat, chimpanzee, gorilla, white-cheeked gibbon, rhesus macaque, pig-tailed macaque, and squirrel monkey were used for ancestral reconstruction. In cases where the sequence of the cloned allele was different from the sequence downloaded from databases, the sequenced allele was used. The protein sequences of Olfr1509

from the 17 species were aligned with MEGA5, and a phylogenetic tree was constructed with the neighbor-joining algorithm using a bootstrap cutoff at 1000. After removing gaps and stop codons in the aligned sequences, ancestral reconstruction was performed with the CODEML program using the tree model in the PAML4.8 software package (Yang 1997, 2007). See Supplementary Figure S14 for putative ancestral sequences.

Plasmid construction

The first 20 amino acids of human rhodopsin (N-MNGTEGPNF YVPFSNATGVVR-C) were inserted between the *Nhe*I and *Eco*RI sites in the mammalian expression vector, pCI. All orthologous sequences of Olfr1509, Olfr1019, and Olfr15 were amplified with open reading frame-flanking primers (Supplementary Table S1) and PrimeSTAR DNA polymerase (TaKaRa). Double-stranded PCR products were column purified using PCR Product Purifying Kit (Generay Biotech) and then cut with *Mlu*I (TaKaRa) and *Not*I (TaKaRa) to insert into the pCI vector. Olfr1509 and Olfr1019 mutants were generated by site-directed mutagenesis through overlap-extension PCR from existing clones. Protein sequences of the hypothetical ancestors were generated by sequential mutageneses from the closest existing clones (Supplementary Figures S14; Figure 2A). All clones were verified by sequencing.

Dual-Glo luciferase assay

HEK293T-derived Hana3A cell line (Saito et al. 2004) were grown in minimum essential medium (HyClone) containing 10% fetal bovine serum (FBS; Gibco) at 37 °C with 5% CO_2. Hana3A cells were plated onto 96-well plates (Greiner). After 18–24 h, transfection was performed. For each 96-well plate, 1 μg of CRE-Luc, 1 μg of pRL-SV40, 5 μg of OR, and 1 μg of mRTP1S were transfected. Plasmid DNA was transfected using Lipofectamine2000 (Invitrogen). At 18–24 h after transfection, the medium was replaced with CD293 chemically defined medium (Gibco), and then the cells were incubated for 30 min at 37 °C with 5% CO_2. The medium was then replaced with various concentrations of MTMT plus copper ions dissolved in CD293 (Invitrogen) and incubated for 4 h at 37 °C with 5% CO_2. The Dual-Glo Luciferase Assay System (Promega) was then used, following the manufacturer's protocol for measuring chemiluminescence.

Flow cytometry

Hana3A cells were seeded in 6-well plates (Greiner) and then transfected with 1.5 μg of OR DNA or pCI and 0.3 μg mRTP1S expression vector per well. As a control for transfection efficiency, 0.3 μg of a green fluorescent protein (GFP) expression vector was transfected per well. Twenty-four-hour post-transfection, the cells were dissociated in a staining and washing solution for flow cytometry (phosphate-buffered saline containing 2% FBS and 15 mM NaN_3) and transferred to a tube for incubation with the anti-rhodopsin antibody (EMD Millipore) and then with phycoerythrin-conjugated donkey anti-mouse IgG (Jackson ImmunoResearch Laboratories, Inc.). Fluorescence was analyzed using Gallios Flow Cytometer (Beckman Coulter).

Data analysis

Data were analyzed with Microsoft Excel 2007 and GraphPad Prism 5. Normalized luciferase activity was calculated by the formula [luc(N) – luc(lowest)]/[luc(highest) – luc(lowest)], where luc(N) = luminescence of firefly luciferase divided by luminescence of *Renilla* luciferase of a certain well; luc(lowest) = lowest luminescence of firefly luciferase divided by luminescence of *Renilla* luciferase of several column of a plate or a plate, or a set of plates; and luc(highest) = highest luminescence of firefly luciferase divided by luminescence of *Renilla* luciferase of a plate or a set of plates. We note that the EC_{50} value of a given receptor can vary between experiments due to varying assay conditions, but the relative sensitivities of the receptor orthologs and mutants remain the same.

Homology modeling

The initial coordinates of the Olfr1509 were taken from the previously reported Olfr1509 model (Sekharan et al. 2014). Such a model of Olfr1509 was prepared with the software package Modeler 9v7 (www.salilab.org/modeller), using the X-ray structure of human M2 muscarinic acetylcholine receptor bound to an antagonist (Protein Data Bank ID: 3UON at 3.0 Å) as a template (Haga et al. 2012).

The homology model of Olfr1019 was built analogously, using the X-ray structure of human M2 muscarinic acetylcholine receptor as a template, because it is the reported crystal structure with highest sequence similarity. Supplementary Figure S10 shows the alignment of primary sequences for the human M2 muscarinic receptor (Haga et al. 2012) and the mouse OR Olfr1019.

Supplementary Figure S11 shows the superposition of structures corresponding to the sequence alignment of transmembrane (TM) regions of Olfr1019 (red) and human M2 muscarinic receptor (blue). The TMHMM server (http://www.cbs.dtu.dk/services/TMHMM/) was utilized to obtain the TM domains by employing the transmembrane hidden Markov model analysis, as applied to model Olfr1509 (Sekharan et al. 2014). As shown in Supplementary Figure S12, the amino acid residues of Olfr1019 with a posterior TM probability greater than 0.1 were assigned to the transmembrane domain.

QM/MM models of Olfr1509 and Olfr1019

QM/MM models of Olfr1509 and Olfr1019 were obtained by geometry optimization of the homology models, as previously reported for the human OR OR2T11 (Li et al. 2016) and the mouse OR Olfr1509 (Sekharan et al. 2014). Starting with the coordinates of the Olfr1509 and Olfr1019 structures as obtained for the homology models of Olfr1509 and Olfr1019, the QM/MM structures were prepared by assigning the bond orders, adding hydrogen atoms, and establishing disulfide bonds with the preparation wizard in Maestro (Maestro 2015). The protonation states for all titratable residues were determined at neutral pH according to PROPKA calculations (Sastry et al. 2013) as implemented in the Schrodinger's Maestro v.10.2 software package (Maestro 2015). Cavities accessible to solvent were filled with water molecules, and a copper ion was coordinated to the putative active site identified by the most favorable interactions. The resulting structures were relaxed via a 3-step optimization procedure to minimize structural changes and preserve the natural shape of the protein. Full optimization based on the AMBER96 force field level (Cornell et al. 1995) was followed by re-optimization using the 2-layer ONIOM scheme with electronic embedding (Vreven et al. 2003) as implemented in Gaussian09 (Frisch et al. 2009). The QM layer of Olfr1019 included the Cu(I) ion, key residues at the binding site (R260, K269, and C254 for Olfr1509 and C203, M256, and R261 for Olfr1019) and the MTMT ligand treated at the DFT/M06-L level of theory (Zhao and Truhlar 2006, 2008). The Stuttgart 8s7p6d2f and 6s5p3d2f ECP10MWB contracted pseudopotential basis set (Andrae et al. 1990) was applied for Cu, whereas the 6-31G(d) basis set (Wiberg 1986) was applied for all other atoms in

the QM layer. The MM layer included the rest of the protein modeled according to the AMBER96 molecular mechanics force field. The interface between the QM and MM layers was treated using the standard hydrogen-link atom scheme (Bakowies and Thiel 1996).

Results

MTMT is a semiochemical that plays an important role in mouse reproduction (Lin et al. 2005). Whether there are other receptors responsible for MTMT perception, whether the copper enhancement effect is essential for the animal's sensitive detection of MTMT, and whether this copper enhancement effect is mouse specific are still unknown. To address these questions, we first performed a high-throughput screening aimed at finding mouse MTMT receptors in addition to Olfr1509. We identified another MTMT receptor, Olfr1019, which responded to MTMT (Supplementary Figure S1). Similar to Olfr1509, we found the response to MTMT by Olfr1019 was significantly enhanced by copper addition (Figure 1B). The presence of a copper effect in Olfr1509 and Olfr1019 is contrasted with a third mouse receptor, Olfr15, which also responded to MTMT, but did not show a copper effect (Duan et al. 2012).

We then blasted the GenBank database for orthologs of mouse MTMT receptors in other mammalian species. Intact sequences for Olfr1509, Olfr1019, and Olfr15 are present in a few different species, such as rat, hamster, pig, horse, and cow. We also found that 1 or more of the 3 receptors became pseudogenized in certain species. In total, we were able to clone 8, 10, and 10 mammalian orthologs for Olfr1509, Olfr1019, and Olfr15, respectively.

We next used a heterologous OR expression system to test the function of these orthologs. We found that the function of all 3 receptors changed at least a few times during evolution: for Olfr1509, some of the orthologs, including pig, rabbit, hamster, cat, and horse, exhibited similar functions as mouse Olfr1509. Importantly, all of these functional orthologous ORs showed a copper effect. Other orthologs, including rat, cow, and human, as well as some nonhuman primate species did not respond to MTMT, with or without copper (Figures 1A,D; Supplementary Figure S2). For Olfr1019, although the human ortholog did not respond to MTMT, the others, including rat, hamster, guinea pig, rabbit, pig, cow, dog, cat, and horse, responded to MTMT and exhibited a copper effect at the same time, similar to the case of Olfr1509 (Figure 1B,D). Finally, for Olfr15, of the 11 orthologs tested, 5 orthologs showed total loss-of-function phenotypes, including guinea pig, cow, horse, cat, and human, whereas dog, pig, rabbit, hamster, and rat responded to MTMT, but all without a copper effect (Figure 1C,D). Notably, among the orthologs of the 2 receptors with a copper effect, we found that all Olfr1019 orthologs except for human exhibited MTMT response with a copper effect. In contrast, Olfr1509 ortholog functions were far more variable. For example, guinea pig and dog Olfr1509 orthologs were pseudogenized, whereas rat and cow Olfr1509 orthologs showed complete loss-of-function. Also, we noticed that the human orthologs of the 3 receptors were all nonfunctional. From a high-throughput screening for human receptors for MTMT, we found a receptor (OR2W1) that could respond to MTMT (Supplementary Figure S3). A broadly tuned OR, OR2W1, responds to a panel of odorants with different structures (Saito et al. 2009). However, the response of OR2W1 to MTMT exhibited no significant difference with and without copper added (Supplementary Figure S4).

With the 3 known MTMT mouse receptors, we hypothesize that amino acid residues crucial for receptor activation and copper effect must be conserved in Olfr1509 and Olfr1019, but not in Olfr15. For the 2 former receptors, these residues should be present in the functional orthologs, whereas mutated in the nonfunctional ones. Previously, as a step toward the elucidation of the activation mechanisms of the MTMT receptors, we identified 3 residues in Olfr1509, H105, C109, and N202 that are involved in binding to the copper–MTMT complex (Sekharan et al. 2014). On examination of the orthologous sequences, we found that all 3 sites are conserved in the 9 Olfr1509 orthologs (Supplementary Figure S5), although these orthologs exhibit different functions against MTMT/Cu. Moreover, these 3 sites are not conserved in either Olfr1019 or Olfr15 (Supplementary Figure S6). We conclude that there must be other residues responsible for copper binding and for the functional differences among the 3 receptors and among the orthologs.

In order to capture additional copper/MTMT-binding sites, we employed a branch-specific approach to focus on lineages of closely related species that had recently experienced functional changes in evolution. In this respect, the Olfr1509 rodent lineage presents an excellent example because the orthologs exhibited different functions (Figure 1A,D). The Olfr1509 rat ortholog, rat Olfr1644, does not respond to MTMT and shows no copper effect even when it shares 95% sequence identity with mouse Olfr1509. The hamster Olfr1509 ortholog, on the other hand, retains the ability to respond to MTMT with a copper effect, but has a decreased function compared with mouse Olfr1509.

We next investigated whether the presence or absence of receptor function/copper effect is ancestral. We performed ancestral reconstruction to obtain the hypothetical ancestral sequences for mouse and rat (Ancestor MR) and for mouse, rat, and hamster (Ancestor MRH), using a maximum likelihood algorithm as implemented in the PAML4.8 package (Yang 1997, 2007). We then cloned these putative ancestral receptors by mutating sequentially from rat, which differs from Ancestor MR by 5 amino acids, and from hamster, which differs from Ancestor MRH by 4 amino acids (Figure 2A; Supplementary Figure S14). We found that both ancestors were functional (Figure 2B), pointing to a change in receptor function from Ancestor MR to rat. Of all the 5 single mutants cloned from rat, 2 mutants, W260R and S297A, differed from the wild-type rat ortholog and showed response to MTMT with the addition of copper. Although the S297A mutant exhibited only a slight increase, the W260R mutation could undoubtedly restore the function lost in rat Olfr1643. Conversely, the mouse Olfr1509 R260W mutant showed a complete loss-of-function phenotype, with or without copper (Figure 3A). In addition, 2 other Olfr1509 mutants, R260H (mutated according to the nonfunctional cow Olfr1509 ortholog, which has H260; Supplementary Figure S5) and R260A, exhibited decreased function and total loss-of-function, respectively.

To further explore the role of the R260 residue in the copper-enhanced MTMT response, we focused on its conservation in all 3 mouse MTMT receptors. We found that the R260 residue is conserved in mouse Olfr1019 (R261), which shows a copper effect, but not in mouse Olfr15 (L261), which exhibits no copper effect (Supplementary Figure S6). R261 is conserved in all 11 Olfr1019 orthologs, of which all 10 nonhuman receptors responded to MTMT with a copper effect. The human Olfr1019 ortholog, OR5AR1, similar to the human orthologs of Olfr1509 and Olfr15, however, showed a total loss-of-function phenotype. Furthermore, similar to Olfr1509, various R261 mutants of Olfr1019, R261W, R261H, and R261A showed total loss-of-function phenotypes (Figure 3A), indicating possible roles of this residue in receptor function involving copper or in receptor function in general.

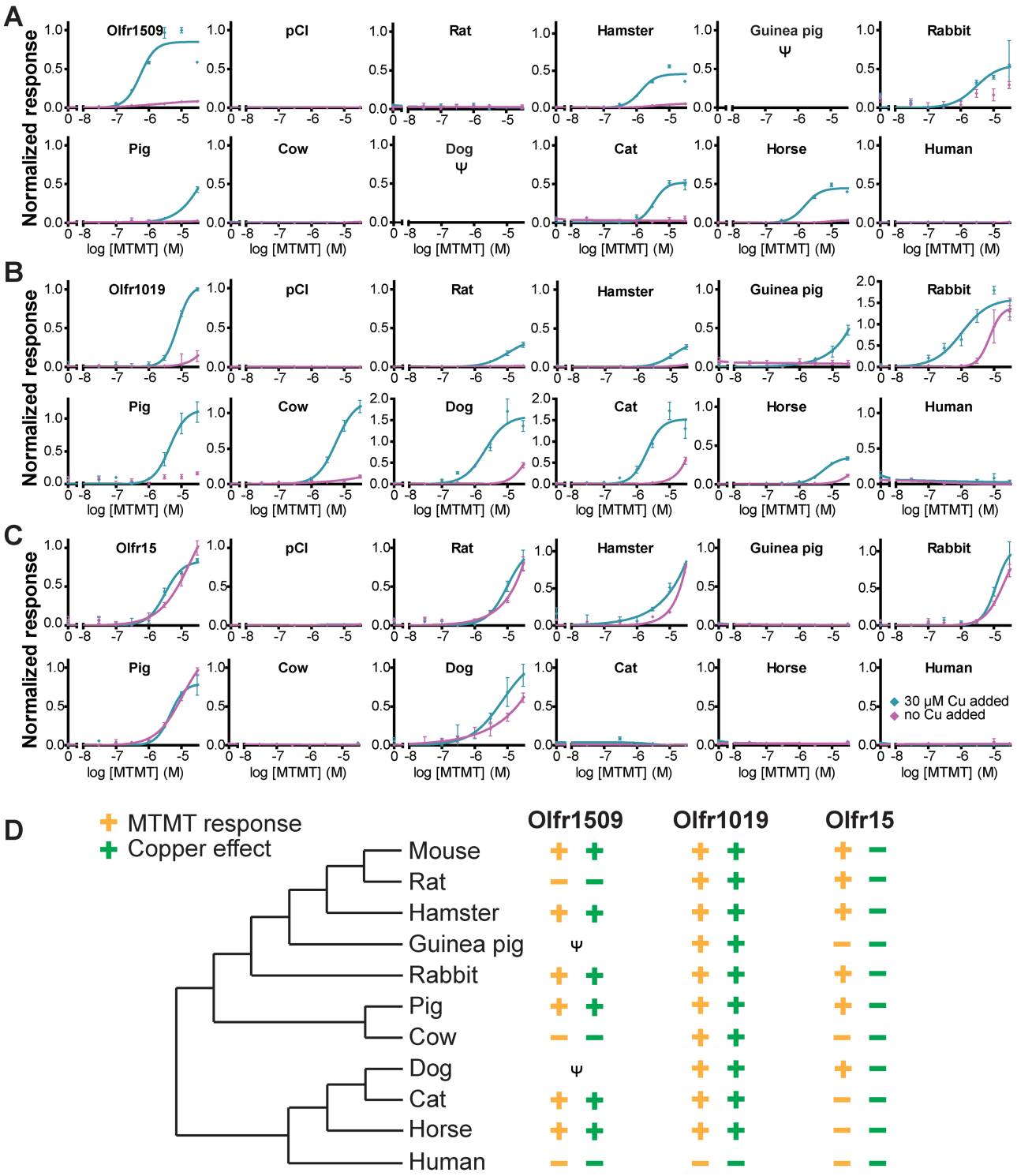

Figure 1. Copper effect co-occurs with the ability to respond to MTMT. Mammalian orthologs of (**A**) Olfr1509, (**B**) Olfr1019, and (**C**) Olfr15 responded differently to MTMT with or without a copper effect. The *y* axis represents mean luciferase activity ± SEM ($N = 3$). All responses were normalized to the highest response of the corresponding mouse orthologs. (**D**) A diagram summarizing the function of the orthologs of the 3 mouse MTMT receptors on a cladogram showing the widely accepted evolutionary relationships among the species. Pseudogenized Olfr1509 orthologs in guinea pig and dog are indicated with a "Ψ".

Finally, we investigated the mechanism of how the R260/R261 site affects receptor function. One route is by affecting receptor folding and/or trafficking to the cell-surface membrane. We found that of all Olfr1509 orthologs tested, rat Olfr1643 and cow OR4E2-like are not expressed on the cell-surface membrane (Supplementary Figure S7A). Olfr1019 orthologs showing different cell-surface expression all conserve R261 (Supplementary Figure S7B), indicating there are other important residues or different mechanisms for the folding and/or trafficking of these 2 orthologous receptor groups. In addition, we also found that the cell-surface expression of the

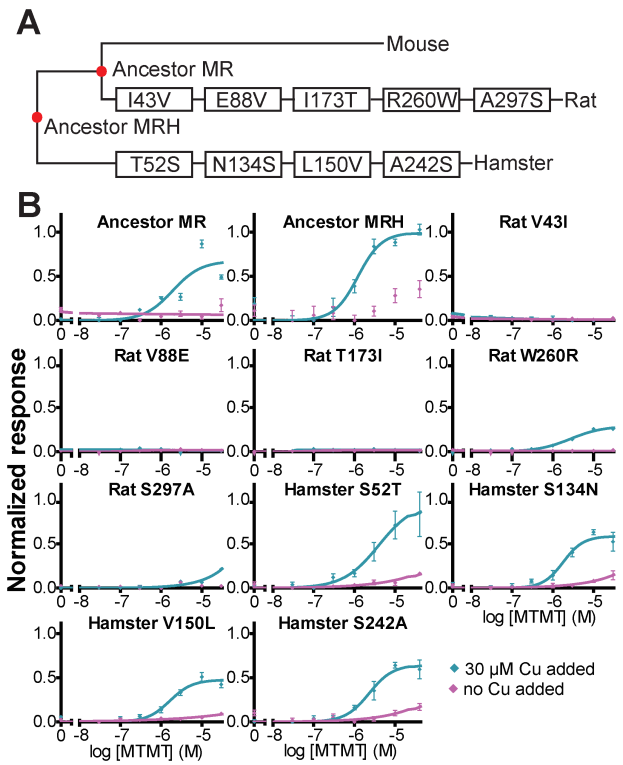

Figure 2. Single mutations contribute to functional variations in the rodent lineage of Olfr1509. (**A**) A cladogram showing the cloned rodent orthologs with all amino acid changes from each of the reconstructed ancestors to rat and hamster indicated in boxes. Dots indicate ancestral nodes "Ancestor MR" and "Ancestor MRH," which stand for the ancestor of mouse and rat and the ancestor of mouse, rat, and hamster, respectively. (**B**) The reconstructed ancestors and single mutants from rat and hamster showed different MTMT response and copper effect with the rat W260R mutation restoring ancestral function. The *y* axis represents mean luciferase activity ± SEM ($N = 3$). All responses were normalized to the highest response of Olfr1509.

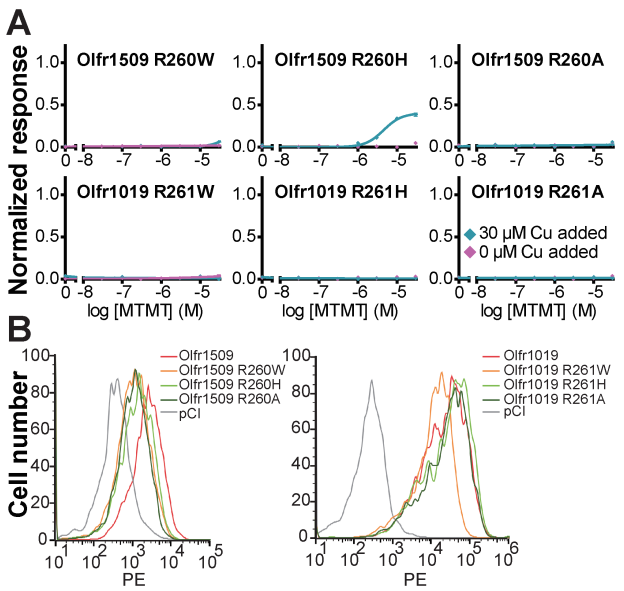

Figure 3. R260/R261 may be involved in copper/MTMT binding in Olfr1509 and Olfr1019. (**A**) Olfr1509 R260 mutants and Olfr1019 R261 mutants exhibit reduced function or total loss-of-function phenotypes. The *y* axis represents mean luciferase activity ± SEM ($N = 3$). All responses were normalized to the highest response of the corresponding wild-type receptors. (**B**) Cell-surface expression of Olfr1509 R260 and Olfr1019 R261 mutants remain relatively unaffected compared with that of the wild-type receptors. The *x* axis indicates the intensity of phycoerythrin (PE) signal in the GFP-positive cell population.

Olfr1509 R260 mutants, as well as the Olfr1019 R261 mutants, were not significantly different from that of the corresponding wild-type receptors (Figure 3B), excluding the impaired cell-surface expression as a cause for receptor malfunction. An alternative possibility is that R260/R261 may play an important role in the activation of the receptors by the MTMT–copper complex.

Structural modeling

Figure 4A,B shows the structural models of Olfr1509 and Olfr1019, respectively. The models share common structural features, including a highly conserved disulfide S–S bond, and provide important insights into the odorant-binding sites. Amino acid residues C179 and C97 form the S–S bond, which is critical for the receptor's structural stability.

The structural analysis suggests the presence of 2 binding sites (site 1 and site 2) in Olfr1509, separated by about 6.0 Å (Supplementary Figure S8). An earlier study of Olfr1509, supports ligand-binding to one of these sites (site 1), located near the extracellular domain (Sekharan et al. 2014). Site 1 involves Cu(I) coordinated to the heteroatoms N, S, and O of amino acid residues H_{105}, C_{109}, and N_{202}, respectively. Cu(I) adopts a tetrahedral coordination with N_{H105} and S_{C109} and a weak interaction with O_{N202} in the absence of a ligand (Sekharan et al. 2014). In contrast, site 2 involves residues C254 and R260 from TM6 near the top of TM6 and K269 from TM7. Analogous to site 1, Cu(I) forms a trigonal planar configuration by coordination to the heteroatoms S_{C254}, N_{R260}, and N_{K269} with distances Cu-S_{C254}, Cu-N_{R260}, and Cu-N_{K269} of 2.16, 1.99, and 2.27 Å, respectively (Supplementary Figure S9A). We note that ligand binding induces coordination rearrangements. We find that the Cu-N_{K269} distance increases to 2.77 Å on MTMT (thiolate form) binding, forming a distorted tetrahedral configuration with the distances Cu-S_{MTMT}, Cu-S_{C254}, Cu-N_{R260}, and Cu-N_{K269} of 2.32, 2.24, 2.01, and 2.77 Å, respectively (Figure 4C).

Similar to Olfr1509, the binding site in Olfr1019 is located near the extracellular domain (Figure 4B). The binding site involves Cu(I) coordinated to amino acid residues S_{C203}, N_{R261}, and N_{M256}. Cu(I) forms trigonal planar geometry by coordination to the heteroatoms S_{C203}, N_{R261}, and N_{M256}, with distances Cu-S_{C203}, Cu-N_{R261}, and Cu-N_{M256} of 2.28, 1.96, and 2.30 Å, respectively (Supplementary Figure S9B). These bond lengths increase to 2.25, 2.27, and 2.92 Å, respectively, on MTMT binding as a thiolate, with a 2.26 Å bond length for the Cu-S_{MTMT} distance (Figure 4D). The significant elongation of the Cu-N_{M256} bond suggests a conformational change at the active site triggered upon ligand binding.

Site-directed mutagenesis combined with the analysis of activation profiles are consistent with the active sites suggested by QM/MM modeling, showing a lack of response to MTMT when mutating amino acid residues responsible for Cu binding. Among the Olfr1509 mutants, C254S and K269A showed a decrease in response, whereas K269H exhibited total loss-of-function. Furthermore, Olfr1019 C203S exhibited a total loss-of-function phenotype, whereas Olfr1019 M256A showed a decreased response (Figure 5).

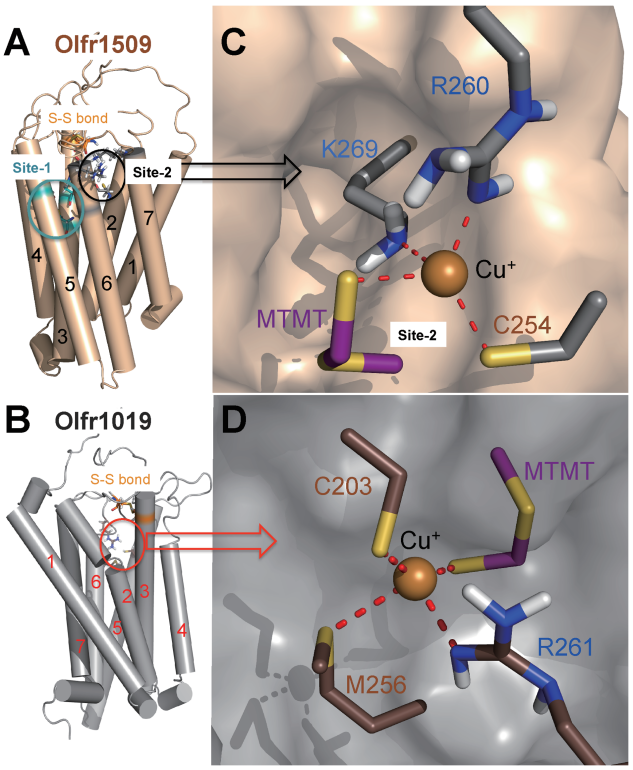

Figure 4. QM/MM modeling reveals metal-binding sites in Olfr1509 and Olfr1019. (**A**) Olfr1509 homology model. Two binding sites are shown as cyan dotted and solid circles. The disulfide (S–S) bond is shown on the top of the model. (**B**) Olfr1019 homology model. The disulfide (S–S) bond is shown as an orange stick. The red solid circle represents the binding site. (**C**) QM/MM optimized model of Olfr1509 with MTMT. The distance between Cu^+ and the S_{MTMT} (thiolate form), S_{C254}, N_{R260}, and N_{K269} are 2.32, 2.24, 2.01, and 2.77 Å, respectively. (**D**) QM/MM optimized ligand-binding site in Olfr1019. The distance between Cu^+ and the S_{MTMT} (thiolate form), S_{C203}, N_{R261}, and N_{M256} are 2.26, 2.25, 2.27, and 2.92 Å, respectively.

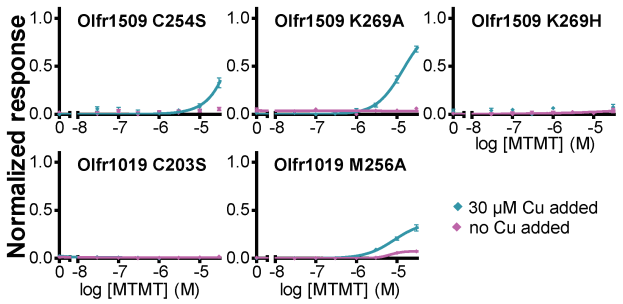

Figure 5. Olfr1509 and Olfr1019 mutant functions. Olfr1509 C254S, Olfr1509 K269A, and Olfr1019 M256A exhibited decreased functions, whereas Olfr1509 K269H and Olfr1019 C203S showed total loss-of-functions. The *y* axis represents mean luciferase activity ± SEM ($N = 3$). All mutant functions were normalized to the highest response of the corresponding wild-type receptors.

Discussion

Thiols and other metal-coordinating chemicals play important roles in the life of mammals that have in turn evolved elaborate yet precise detection and response mechanisms for these compounds. We previously discovered the copper-requiring detection of MTMT by Olfr1509. Here, we characterize the functional variation in the different MTMT receptor orthologs and identify additional sites important for receptor function.

Sensitive detection of metal-coordinating odorants

Several metal-coordinating odorants are central to the different aspects of organismal behaviors, including reproduction, social communication, feeding, and predator avoidance. Besides MTMT, trimethylamine is another attractive and potentially metal-coordinating compound in male mouse urine (Hancock and Martell 1988; Gavaghan McKee et al. 2006; Li et al. 2013). Of carnivorous origin, trimethylthiazoline and 2-phenylethylamine are odors that repel rodent species (Sabelli et al. 1975; Morrow et al. 2000; Buron et al. 2007; Ferrero et al. 2011). Sulfur- and nitrogen-containing odors are found in body-borne odors of primates, suggesting that they may play important roles in social communication (Laska et al. 2007). In humans, thiols and amines such as trimethylamine are associated with bad breath (Yaegaki and Suetaka 1989; Bollen and Beikler 2012) and sweat (Troccaz et al. 2004, 2009; Loos et al. 2017). Other mammals such as the flower-visiting bats in the tropical lowland rain forests of Costa Rica are specifically attracted by sulfur odor-containing flowers, with MTMT being one of the odorous components (von Helversen et al. 2000). It is worth noting that our in vitro experiments showed that the orthologous ORs of both Olfr1509 and Olfr1019 in the Old World bat species, *Myotis lucifugus*, could also respond to MTMT and showed a copper effect (Supplementary Figure S13). Also of food origin, thiols and amines are present as a result of protein degradation in putrid food. Sensitive detection and avoidance of these volatile chemicals effectively prevents food poisoning (Block 1978; Laska et al. 2007). All of these examples underscore the evolutionary significance of the sensitive detection of metal-coordinating ligands and hence the selective pressure on their respective receptors in different species. Other than mouse and certain bat species, it is not known whether MTMT is present in the urine, or any other aspects of the life, of other mammalian species with positive receptor function. Future chemical analysis of urine samples and behavioral assays of selected rodent species may help to correlate receptor function with species-specific behaviors.

The requirement for sensitive detection is further emphasized by the locale of MTMT receptor expression. In addition to their expression in the main olfactory epithelium (MOE), both Olfr1509 and Olfr15 express widely in the mouse SO (Kaluza et al. 2004; Tian and Ma 2004, 2008; Duan et al. 2012). The SO is a cluster of cells located on the nasal septum ventral to the MOE and caudal to the vomeronasal organ (Tian and Ma 2004; Breer et al. 2006; Barrios et al. 2014). Because of its position in the nasal cavity, it was hypothesized that the SO is automatically exposed to airflow during normal respiration in a more efficient way than the MOE (Rodolfo-Masera 1943). As an accessory olfactory organ involved in sexual and social behaviors, the SO responds to a broad range of odor stimuli, possibly with sensitivities even higher than MOE (Marshall and Maruniak 1986).

Although MTMT and other related thioether thiols are capable of coordinating to metals, especially copper, the response to MTMT by ORs does not always require copper. Such lack of metal requirement is also preserved in evolution, as exemplified by the case of Olfr15, the functional orthologs of which responded to MTMT without copper. It is worth noting that Olfr15 belongs to the MOR256 family, one of the largest mouse OR families, which has at least 37 functional family members (Zhang and Firestein 2002; Li et al. 2012). Several MOR256 family members, Olfr124, Olfr263,

and Olfr15, are identified as broadly tuned receptors, capable of responding to a wide variety of linear aliphatic, cyclic, and aromatic structures, with sulfur-containing compounds being one of the many classes of odorants that could activate them (Grosmaitre et al. 2009; Nara et al. 2011; Li et al. 2012; Tazir et al. 2016). In contrast to the sensitive detection by Olfr1509 and Olfr1019 with the aid of copper ion, broadly tuned receptors such as Olfr15 could ensure a basal level of response to this crucial pheromone.

In addition to the previously identified Olfr1509 and Olfr15, we found an additional mouse OR, Olfr1019, that responds robustly to MTMT. Similar to Olfr1509, Olfr1019 requires copper for the sensitive detection of MTMT. There is a strong possibility that there may be other mouse MTMT receptors yet to be identified. Future experiments involving screening assays over the complete mouse OR repertoire may yield additional candidate receptors. Furthermore, by using a HEK293T-based OR heterologous expression system to screen for MTMT receptors and evaluate receptor pharmacology, it is possible that receptor sensitivity and odor tuning may be different from that of the in vivo conditions due to the lack of endogenous molecules that are present in native olfactory sensory neurons and the absence of soluble proteins and enzymatic conversions occurring in the nasal mucus (Heydel et al. 2013; Hanser et al. 2017). Recent technologies featuring high-throughput in vivo assays may help to reveal additional MTMT receptors relevant to organismal responses.

Functional sites in MTMT receptor activation

Several amino acid residues, including histidine, cysteine, methionine, glutamine, asparagine, and so on, are reported to have copper-binding abilities (Karlin and Zhu 1996). Generally, clusters containing 2 or more of these amino acids, which are separated by less than 4 amino acids, are believed to be involved in the coordination of multiple residues to the metal ion. Wang et al. (2003) showed that a short synthetic peptide sequence HACKE could bind to Cu^{2+}, Zn^{2+}, or Ni^{2+} and undergo a conformational change. They thus proposed a consensus metal-binding site HXXC[DE] (X being any amino acid) in the extracellular loop of human ORs between transmembrane domains 4 and 5 (Wang et al. 2003). Olfr1509, although exhibiting a prominent copper effect, lacks this special peptide sequence in the second extracellular loop. By surveying all His, Cys, and Met residues in Olfr1509, we preliminarily reported 1 site, H105, found between the second to fifth transmembrane domains, close to the extracellular side, that could play an important role in copper binding in Olfr1509 (Duan et al. 2012). Further mutagenesis studies and QM/MM calculations allowed us to elucidate a copper binding pocket in Olfr1509 consisting of H105/C109/N202 (Sekharan et al. 2014).

In addition to the previously identified copper-binding sites, in this study, we identified for the first time the residue R260/R261, which is located in the sixth transmembrane domain (TM6) and is shared by the functional orthologs and ancestors of Olfr1509 and Olfr1019. TM6 is widely recognized as an OR–ligand-binding region, with a highly conserved amino residue, tyrosine, playing a crucial role in ligand binding. The hydroxyl group on the tyrosine side chain is reported to be very important in the function of both the rat OR I7 (Y264) (Kurland et al. 2010) and the mouse OR OREG (Y260) (Baud et al. 2011). This site is also conserved in Olfr1509 and Olfr1019 (Y258/Y259), only one residue away from R260/R261. It is probable that R260 could be directly involved in copper binding or indirectly through hydrogen-bonding networks within the receptor cavity.

In previous modeling work of the mouse OR MOR912-93 (Olfr154), Gaillard et al. (2004) cloned a series of MOR912-93 orthologs and tested the functions of these orthologs against 2-heptanone and 3-heptanone. They found that the human and orangutan orthologs did not respond to either ligand (Gaillard et al. 2004; Figure 2A); interestingly, R261 is not conserved in these 2 orthologs like the other functional MOR912-93 orthologs. Note that this is the only residue in addition to the R122C (human) and R121H (orangutan) mutations in the MAYDRY motif that differs from the rest of the functional orthologs (Gaillard et al. 2004; Figure 1A). This agrees with our finding that Olfr1509 orthologs that lack R260, the corresponding site to MOR912-93 R261, exhibit a total loss-of-function phenotype against MTMT/Cu. It is highly probable that R261 in this receptor may be vital for MOR912-93 ligand binding. However, further functional analysis and modeling work is needed to validate this proposal. Alternatively, R260/R261, being near the ligand-binding pocket of Olfr1509 and Olfr1019, may be involved in other aspects of receptor activation, such as a hydrogen-bonding network. Our computational modeling analysis suggests that the R260/R261 residue in Olfr1509/Olfr1019 coordinates to Cu(I) both in the presence and in the absence of MTMT. MTMT binding induces elongation of the coordination bonds Cu-N_{K269} and Cu-N_{M256} in Olfr1509 and Olfr1019, respectively, suggesting a significant conformational change on ligand binding. It is also important to note that the R260/R261 residue is essential for the observed copper effect and response to odorant (MTMT) binding. Finally, different activation mechanisms may exist for receptors that do not involve metal in MTMT binding. We noticed that the residues corresponding to the ones located close to the proposed MTMT-binding sites of Olfr1509 and Olfr1019, that is, Y102 and Y257 in Olfr15, are not conserved. Future computational and biological studies may help unveil the key residues in non-metal-requiring sulfur receptors.

Supplementary Material

Supplementary data are available at *Chemical Senses* online.

Funding

This study was supported by National Natural Science Foundation of China (31070972); the Program for Innovative Research Team of Shanghai Municipal Education Commission; the Shanghai Eastern Scholar Program (J50201); the National Basic Research Program of China (2012CB910401); the Shanghai Natural Science Foundation (16ZR1418300) (all to H.Z.); the National Science Foundation (CHE-1465108 to V.S.B.; CHE-1265679 and CHE-1545712 to E.B.); and the Doctoral Innovation Fund Projects from Shanghai Jiaotong University School of Medicine (BXJ201303 to R.Z.).

Acknowledgments

We thank Dr David A. Ray for generously providing the bat (*Myotis lucifugus*) genomic DNA. V.S.B. acknowledges supercomputer time from NERSC and the Yale High Performance Computing Center.

References

Adipietro KA, Mainland JD, Matsunami H. 2012. Functional evolution of mammalian odorant receptors. *PLoS Genet*. 8:e1002821.

Altenhoff AM, Dessimoz C. 2012. Inferring orthology and paralogy. *Methods Mol Biol*. 855:259–279.

Altenhoff AM, Studer RA, Robinson-Rechavi M, Dessimoz C. 2012. Resolving the ortholog conjecture: orthologs tend to be weakly, but significantly, more similar in function than paralogs. *PLoS Comput Biol*. 8:e1002514.

Andrae D, Häußermann U, Dolg M, Stoll H, Preuß H. 1990. Energy-adjusted ab initio pseudopotentials for the second and third row transition elements. *Theor Chim Acta*. 77:123–141.

Araneda RC, Kini AD, Firestein S. 2000. The molecular receptive range of an odorant receptor. *Nat Neurosci*. 3:1248–1255.

Bakowies D, Thiel W. 1996. Hybrid models for combined quantum mechanical and molecular mechanical approaches. *J Phys Chem*. 100:10580–10594.

Barrios AW, Núñez G, Sánchez Quinteiro P, Salazar I. 2014. Anatomy, histochemistry, and immunohistochemistry of the olfactory subsystems in mice. *Front Neuroanat*. 8:63.

Baud O, Etter S, Spreafico M, Bordoli L, Schwede T, Vogel H, Pick H. 2011. The mouse eugenol odorant receptor: structural and functional plasticity of a broadly tuned odorant binding pocket. *Biochemistry*. 50:843–853.

Block E. 1978. *Reactions of organosulfur compounds*. New York: Academic Press.

Block E, Batista VS, Matsunami H, Zhuang H, Ahmed L. 2017. The role of metals in mammalian olfaction of low molecular weight organosulfur compounds. *Nat Prod Rep*. 34:529–557.

Bollen CM, Beikler T. 2012. Halitosis: the multidisciplinary approach. *Int J Oral Sci*. 4:55–63.

Bozza T, Vassalli A, Fuss S, Zhang JJ, Weiland B, Pacifico R, Feinstein P, Mombaerts P. 2009. Mapping of class I and class II odorant receptors to glomerular domains by two distinct types of olfactory sensory neurons in the mouse. *Neuron*. 61:220–233.

Breer H, Fleischer J, Strotmann J. 2006. The sense of smell: multiple olfactory subsystems. *Cell Mol Life Sci*. 63:1465–1475.

Buck L, Axel R. 1991. A novel multigene family may encode odorant receptors: a molecular basis for odor recognition. *Cell*. 65:175–187.

Buron G, Hacquemand R, Pourie G, Lucarz A, Jacquot L, Brand G. 2007. Comparative behavioral effects between synthetic 2,4,5-trimethylthiazoline (TMT) and the odor of natural fox (*Vulpes vulpes*) feces in mice. *Behav Neurosci*. 121:1063–1072.

Chatelain P, Veithen A, Wilkin F, Philippeau M. 2014. Deorphanization and characterization of human olfactory receptors in heterologous cells. *Chem Biodivers*. 11:1764–1781.

Chen X, Zhang J. 2012. The ortholog conjecture is untestable by the current gene ontology but is supported by RNA sequencing data. *PLoS Comput Biol*. 8:e1002784.

Conant GC, Wolfe KH. 2008. Turning a hobby into a job: how duplicated genes find new functions. *Nat Rev Genet*. 9:938–950.

Cornell WD, Cieplak P, Bayly CI, Gould IR, Merz KM, Ferguson DM, Spellmeyer DC, Fox T, Caldwell JW, Kollman PA. 1995. A second generation force field for the simulation of proteins, nucleic acids, and organic molecules. *J Am Chem Soc*. 117:5179–5197.

Crabtree RH. 1978. Copper (I): a possible olfactory binding site. *J Inorg Nucl Chem*. 40:1453.

Duan X, Block E, Li Z, Connelly T, Zhang J, Huang Z, Su X, Pan Y, Wu L, Chi Q, *et al.* 2012. Crucial role of copper in detection of metal-coordinating odorants. *Proc Natl Acad Sci USA*. 109:3492–3497.

Ferrero DM, Lemon JK, Fluegge D, Pashkovski SL, Korzan WJ, Datta SR, Spehr M, Fendt M, Liberles SD. 2011. Detection and avoidance of a carnivore odor by prey. *Proc Natl Acad Sci USA*. 108:11235–11240.

Firestein S. 2001. How the olfactory system makes sense of scents. *Nature*. 413:211–218.

Forslund K, Pekkari I, Sonnhammer EL. 2011. Domain architecture conservation in orthologs. *BMC Bioinformatics*. 12:326.

Frisch MJ, Trucks GW, Schlegel HB, Scuseria GE, Robb MA, Cheeseman JR, Scalmani G, Barone V, Mennucci B, Petersson GA, *et al.* 2009. *Gaussian 09*. Wallingford (CT): Gaussian, Inc.

Gaillard I, Rouquier S, Chavanieu A, Mollard P, Giorgi D. 2004. Amino-acid changes acquired during evolution by olfactory receptor 912-93 modify the specificity of odorant recognition. *Hum Mol Genet*. 13:771–780.

Gavaghan McKee CL, Wilson ID, Nicholson JK. 2006. Metabolic phenotyping of nude and normal (Alpk:ApfCD, C57BL10J) mice. *J Proteome Res*. 5:378–384.

Grosmaitre X, Fuss SH, Lee AC, Adipietro KA, Matsunami H, Mombaerts P, Ma M. 2009. SR1, a mouse odorant receptor with an unusually broad response profile. *J Neurosci*. 29:14545–14552.

Haga K, Kruse AC, Asada H, Yurugi-Kobayashi T, Shiroishi M, Zhang C, Weis WI, Okada T, Kobilka BK, Haga T, *et al.* 2012. Structure of the human M2 muscarinic acetylcholine receptor bound to an antagonist. *Nature*. 482:547–551.

Hancock RD, Martell AE. 1988. The chelate, macrocyclic, and cryptate effects. *Comment Inorg Chem*. 6:237–284.

Hanser HI, Faure P, Robert-Hazotte A, Artur Y, Duchamp-Viret P, Coureaud G, Heydel JM. 2017. Odorant-odorant metabolic interaction, a novel actor in olfactory perception and behavioral responsiveness. *Sci Rep*. 7:10219.

Hayden S, Bekaert M, Crider TA, Mariani S, Murphy WJ, Teeling EC. 2010. Ecological adaptation determines functional mammalian olfactory subgenomes. *Genome Res*. 20:1–9.

Heydel JM, Coelho A, Thiebaud N, Legendre A, Le Bon AM, Faure P, Neiers F, Artur Y, Golebiowski J, Briand L. 2013. Odorant-binding proteins and xenobiotic metabolizing enzymes: implications in olfactory perireceptor events. *Anat Rec (Hoboken)*. 296:1333–1345.

Kaluza JF, Gussing F, Bohm S, Breer H, Strotmann J. 2004. Olfactory receptors in the mouse septal organ. *J Neurosci Res*. 76:442–452.

Karlin S, Zhu ZY. 1996. Characterizations of diverse residue clusters in protein three-dimensional structures. *Proc Natl Acad Sci USA*. 93:8344–8349.

Katada S, Hirokawa T, Oka Y, Suwa M, Touhara K. 2005. Structural basis for a broad but selective ligand spectrum of a mouse olfactory receptor: mapping the odorant-binding site. *J Neurosci*. 25:1806–1815.

Kurland MD, Newcomer MB, Peterlin Z, Ryan K, Firestein S, Batista VS. 2010. Discrimination of saturated aldehydes by the rat I7 olfactory receptor. *Biochemistry*. 49:6302–6304.

Laska M, Bautista RM, Höfelmann D, Sterlemann V, Salazar LT. 2007. Olfactory sensitivity for putrefaction-associated thiols and indols in three species of non-human primate. *J Exp Biol*. 210:4169–4178.

Li S, Ahmed L, Zhang R, Pan Y, Matsunami H, Burger JL, Block E, Batista VS, Zhuang H. 2016. Smelling sulfur: copper and silver regulate the response of human odorant receptor OR2T11 to low-molecular-weight thiols. *J Am Chem Soc*. 138:13281–13288.

Li J, Haddad R, Chen S, Santos V, Luetje CW. 2012. A broadly tuned mouse odorant receptor that detects nitrotoluenes. *J Neurochem*. 121:881–890.

Li Q, Korzan WJ, Ferrero DM, Chang RB, Roy DS, Buchi M, Lemon JK, Kaur AW, Stowers L, Fendt M, *et al.* 2013. Synchronous evolution of an odor biosynthesis pathway and behavioral response. *Curr Biol*. 23:11–20.

Lin DY, Zhang SZ, Block E, Katz LC. 2005. Encoding social signals in the mouse main olfactory bulb. *Nature*. 434:470–477.

Loos HM, Doucet S, Védrines F, Sharapa C, Soussignan R, Durand K, Sagot P, Buettner A, Schaal B. 2017. Responses of human neonates to highly diluted odorants from sweat. *J Chem Ecol*. 43:106–117.

Maestro. 2015. New York (NY): Schrödinger, LLC.

Marshall DA, Maruniak JA. 1986. Masera's organ responds to odorants. *Brain Res*. 366:329–332.

Moore CH, Pustovyy O, Dennis JC, Moore T, Morrison EE, Vodyanoy VJ. 2012. Olfactory responses to explosives associated odorants are enhanced by zinc nanoparticles. *Talanta*. 88:730–733.

Morrow BA, Redmond AJ, Roth RH, Elsworth JD. 2000. The predator odor, TMT, displays a unique, stress-like pattern of dopaminergic and endocrinological activation in the rat. *Brain Res*. 864:146–151.

Nagashima A, Touhara K. 2010. Enzymatic conversion of odorants in nasal mucus affects olfactory glomerular activation patterns and odor perception. *J Neurosci*. 30:16391–16398.

Nara K, Saraiva LR, Ye X, Buck LB. 2011. A large-scale analysis of odor coding in the olfactory epithelium. *J Neurosci*. 31:9179–9191.

Nehrt NL, Clark WT, Radivojac P, Hahn MW. 2011. Testing the ortholog conjecture with comparative functional genomic data from mammals. *PLoS Comput Biol*. 7:e1002073.

Niimura Y, Matsui A, Touhara K. 2014. Extreme expansion of the olfactory receptor gene repertoire in African elephants and evolutionary dynamics of orthologous gene groups in 13 placental mammals. *Genome Res*. 24:1485–1496.

Niimura Y, Nei M. 2007. Extensive gains and losses of olfactory receptor genes in mammalian evolution. *PLoS One*. 2:e708.

Persaud KC, Marco S, Gutiérrez-Gálvez A. 2013. *Engineering aspects of olfaction*. Boca Raton (FL): CRC Press.

Rodolfo-Masera T. 1943. Sur l'esistenza di un particolare organo olfacttivo nel setto nasale della cavia e di altri roditori. *Arch Ital Anat Embriol*. 48:157–212.

Sabelli HC, Vazquez AJ, Flavin D. 1975. Behavioral and electrophysiological effects of phenylethanolamine and 2-phenylethylamine. *Psychopharmacologia*. 42:117–125.

Saito H, Chi Q, Zhuang H, Matsunami H, Mainland JD. 2009. Odor coding by a mammalian receptor repertoire. *Sci Signal*. 2:ra9.

Saito H, Kubota M, Roberts RW, Chi Q, Matsunami H. 2004. RTP family members induce functional expression of mammalian odorant receptors. *Cell*. 119:679–691.

Sastry GM, Adzhigirey M, Day T, Annabhimoju R, Sherman W. 2013. Protein and ligand preparation: parameters, protocols, and influence on virtual screening enrichments. *J Comput Aided Mol Des*. 27:221–234.

Sekharan S, Ertem MZ, Zhuang H, Block E, Matsunami H, Zhang R, Wei JN, Pan Y, Batista VS. 2014. QM/MM model of the mouse olfactory receptor MOR244-3 validated by site-directed mutagenesis experiments. *Biophys J*. 107:L5–L8.

Tazir B, Khan M, Mombaerts P, Grosmaitre X. 2016. The extremely broad odorant response profile of mouse olfactory sensory neurons expressing the odorant receptor MOR256-17 includes trace amine-associated receptor ligands. *Eur J Neurosci*. 43:608–617.

Tian H, Ma M. 2004. Molecular organization of the olfactory septal organ. *J Neurosci*. 24:8383–8390.

Tian H, Ma M. 2008. Differential development of odorant receptor expression patterns in the olfactory epithelium: a quantitative analysis in the mouse septal organ. *Dev Neurobiol*. 68:476–486.

Touhara K, Vosshall LB. 2009. Sensing odorants and pheromones with chemosensory receptors. *Annu Rev Physiol*. 71:307–332.

Troccaz M, Borchard G, Vuilleumier C, Raviot-Derrien S, Niclass Y, Beccucci S, Starkenmann C. 2009. Gender-specific differences between the concentrations of nonvolatile (R)/(S)-3-methyl-3-sulfanylhexan-1-Ol and (R)/(S)-3-hydroxy-3-methyl-hexanoic acid odor precursors in axillary secretions. *Chem Senses*. 34:203–210.

Troccaz M, Starkenmann C, Niclass Y, van de Waal M, Clark AJ. 2004. 3-Methyl-3-sulfanylhexan-1-ol as a major descriptor for the human axilla-sweat odour profile. *Chem Biodivers*. 1:1022–1035.

Viswaprakash N, Dennis JC, Globa L, Pustovyy O, Josephson EM, Kanju P, Morrison EE, Vodyanoy VJ. 2009. Enhancement of odorant-induced responses in olfactory receptor neurons by zinc nanoparticles. *Chem Senses*. 34:547–557.

Vodyanoy V. 2010. Zinc nanoparticles interact with olfactory receptor neurons. *Biometals*. 23:1097–1103.

von Helversen O, Winkler L, Bestmann HJ. 2000. Sulphur-containing "perfumes" attract flower-visiting bats. *J Comp Physiol A*. 186:143–153.

Vreven T, Morokuma K, Farkas O, Schlegel HB, Frisch MJ. 2003. Geometry optimization with QM/MM, ONIOM, and other combined methods. I. Microiterations and constraints. *J Comput Chem*. 24:760–769.

Wang J, Luthey-Schulten ZA, Suslick KS. 2003. Is the olfactory receptor a metalloprotein? *Proc Natl Acad Sci USA*. 100:3035–3039.

Wiberg KB. 1986. Ab initio molecular orbital theory by W. J. Hehre, L. Radom, P. v. R. Schleyer, and J. A. Pople, John Wiley, New York, 548pp. *J Comput Chem*. 7:379.

Yaegaki K, Suetaka T. 1989. Fractionation of the salivary cellular elements by Percoll density gradient centrifugation and the distribution of oral malodour precursors. *Shigaku*. 77:269–275.

Yang Z. 1997. PAML: a program package for phylogenetic analysis by maximum likelihood. *Comput Appl Biosci*. 13:555–556.

Yang Z. 2007. PAML 4: phylogenetic analysis by maximum likelihood. *Mol Biol Evol*. 24:1586–1591.

Zhang X, Firestein S. 2002. The olfactory receptor gene superfamily of the mouse. *Nat Neurosci*. 5:124–133.

Zhao S, Tian H, Ma L, Yuan Y, Yu CR, Ma M. 2013. Activity-dependent modulation of odorant receptor gene expression in the mouse olfactory epithelium. *PLoS One*. 8:e69862.

Zhao Y, Truhlar DG. 2006. A new local density functional for main-group thermochemistry, transition metal bonding, thermochemical kinetics, and noncovalent interactions. *J Chem Phys*. 125:194101.

Zhao Y, Truhlar DG. 2008. The M06 suite of density functionals for main group thermochemistry, thermochemical kinetics, noncovalent interactions, excited states, and transition elements: two new functionals and systematic testing of four M06-class functionals and 12 other functionals. *Theor Chem Acc*. 120:215–241.

Zhuang H, Chien MS, Matsunami H. 2009. Dynamic functional evolution of an odorant receptor for sex-steroid-derived odors in primates. *Proc Natl Acad Sci USA*. 106:21247–21251.